A&A 456, 451–466 (2006)
DOI: 10.1051/0004-6361:20053063

Astronomy & Astrophysics

Planetary nebulae in the Magellanic Clouds[⋆,⋆⋆]

II. Abundances and element production

P. Leisy[1,⋆⋆⋆] and M. Dennefeld[2]

[1] Isaac Newton Group of telescopes ING/IAC, La Palma, Spain
e-mail: pleisy@ing.iac.es
[2] Institut d'Astrophysique de Paris, CNRS, and Université P. et M. Curie, 98bis Bd Arago, 75014 Paris, France

Received 14 March 2005 / Accepted 31 March 2006

ABSTRACT

Context. We present the second part of an optical spectroscopic study of planetary nebulae in the LMC and SMC. The first paper, Leisy & Dennefeld (1996, A&AS, 116, 96), discussed the CNO cycle for those objects where C abundances were available.
Aims. In this paper we concentrate more on other elemental abundances (such as O, Ne, S, Ar) and their implications for the evolution of the progenitor stars.
Methods. We use a much larger sample of 183 objects, of which 65 are our own observations, where the abundances have been re-derived in a homogeneous way. For 156 of them, the quality of data is considered to be satisfactory for further analysis.
Results. We confirm the difficulty of separating type I and non-type-I objects in the classical He-N/O diagram, as found in Paper I, a problem reinforced by the variety of initial compositions for the progenitor stars. We observed oxygen variations, either depletion via the ON cycle in the more massive progenitor stars, or oxygen production in other objects. Neon production also appears to be present. These enrichments seem to be explained best by recent models, some including overshooting, where fresh material from the core or from burning shells is brought to the surface by the 3rd dredge-up. All the effects appear stronger in the SMC, suggesting a higher efficiency in a low metallicity environment, either because the reaction itself is more efficient or because the increment is more visible when superposed on a low initial quantity.
Conclusions. Neither oxygen nor neon can therefore be used to derive the initial composition of the progenitor star: other elements not affected by processing such as sulfur, argon or, if observed, chlorine, have to be preferred for this purpose. Some objects with very low initial abundances are detected, but on average, the spatial distribution of PNe abundances is consistent with the history of star formation (SF) as derived from field stars in both Clouds.

Key words. planetary nebulae: general – galaxies: Magellanic Clouds – galaxies: evolution – ISM: abundances – stars: abundances

1. Introduction

Planetary nebulae (PNe) are prime targets for studing the chemical evolution of nearby galaxies. This is particularly true for the two Magellanic Clouds, which have a different composition from our own Galaxy, thus allowing the study of metallicity effects. Their distances are known with reasonable accuracy, and thus the physical properties of the PNe can be determined easily; and they are close enough that a large number of PNe have already been identified, therefore giving statistical significance to the derived properties.

In our first paper (Leisy & Dennefeld 1996; hereafter Paper I) we reported our observations of PNe in the Magellanic Clouds, and discussed those objects (16 in LMC and 15 in SMC) for which carbon abundances were available. The present paper discusses the entire sample for which optical observations are available: 65 objects from our own observations, to which we add 118 other PNe already published in the literature. All the data were treated for the first time in a homogeneous way, allowing a global analysis of elemental abundances in the Magellanic Clouds.

At the end of their evolution, intermediate-mass stars pass through an asymptotic giant branch (AGB) phase and experience helium shell flashes (Thermal-Pulse AGB). During these phases, they lose most of their envelopes. These envelopes contain both original, un-processed material and material synthesized in the deep layers of the star, and then dredged-up during the Red Giant and AGB phases. Therefore substantial mass is ejected, which enriches the interstellar medium (ISM) with processed elements such as He, C, N and s-process elements (see for example Renzini & Voli 1981; Iben & Renzini 1983; Dopita & Meatheringham 1991a; Vassiliadis & Wood 1993). But the ISM is also enriched in other, un-processed elements that were incorporated from the ISM at the time the progenitor star was formed, such as O, S, Ar, or Fe, which are elements believed to remain un-processed during the evolution of the PN progenitor star.

For those elements synthesized during the lifetime of their progenitor stars, the study of PNe allows one to determine how the production of chemical elements depends on initial mass or metallicity and how the products are *dredged-up* during the late stages of stellar evolution. Although Kaler et al. (1978), Becker & Iben (1979, 1980), Renzini & Voli (1981), or

⋆ Based on observations made at the European Southern Observatory, La Silla, Chile.
⋆⋆ Tables 3–6, A1 and A2 are only available in electronic form at the CDS via anonymous ftp to
cdsarc.u-strasbg.fr (130.79.128.5) or via
http://cdsweb.u-strasbg.fr/cgi-bin/qcat?J/A+A/456/451
⋆⋆⋆ Part of this work was done while at ESO La Silla, Chile and in Prérebois, Rombach-le-Franc, France.

Sweigart et al. (1989, 1990) have demonstrated reasonable agreement between observations and the dredge-up theory for giant stars, quantitative discrepancies still exist. We showed in Paper I that initial metallicity plays a crucial role in the efficiency of the various reactions and that additional processes, such as Hot Bottom Burning, predicted by theory (Gronewegen & de Jong 1993) were effectively observed. Recent evolution models of intermediate mass stars incorporating this are now available for a direct comparison with observations (Marigo et al. 1996, Marigo 2001 or Marigo et al. 2003).

While PNe play an important role in the chemical evolution of their host galaxies by furnishing helium, carbon, and nitrogen in great quantities, they can also be used to trace the evolution of those elements not affected by processing in their progenitor stars. With masses in the range 1 $M_\odot \leq M_i \leq 8\ M_\odot$, evolution can be traced from PNe over the past 10 billion years, provided the mass of the central star and its initial metallicity are known. The latter is usually derived from oxygen, but in view of the metallicity effects shown in Paper I and the involvement of O in the CNO cycle (as discussed later in this paper), other heavy elements, such as neon, sulfur and argon will also have to be used. Present day abundances in the ISM, used for comparison, are determined from H II regions.

A large sample of objects, with various metallicities and an homogeneous data reduction and determination of abundances such as the one provided here, is therefore crucial to understand the role of the various parameters involved. It will also allow a global analysis of the chemical evolution of the Magellanic Clouds to be compared with the results obtained from H II regions (e.g. by Dufour 1984, 20 objects) and with those obtained from direct studies of a few stellar spectra (Spite et al. 1991; Hill et al. 2000). Such a program is a long-term observational enterprise, and first results have already been presented in various conferences (e.g. in Leisy & Dennefeld 2000).

A short description of the observations and data reduction is given again in Sect. 2, as a reminder from Paper I. The physical parameters for the objects, the abundances determinations, and the corresponding uncertainties are given in Sect. 3. Readers not interested in the details of the derivation of the PNe parameters can go directly to Sect. 4, where the abundance patterns are discussed element by element. Implications for the chemical evolution of the Magellanic Clouds are presented in Sect. 5.

2. Observations and data reduction

The objects observed and named according to the SIMBAD nomenclature were mainly selected from the list of Sanduleak et al. (1978) (SMP LMC or SMP SMC), with a few additions from Henize (1956: LHA-120 Nxx for LMC, LHA-115 Nxx for SMC), Morgan & Good (1992: MGPN LMC N = 1,86), Morgan (1994: [$M94b$] N = 1,54), Morgan & Good (1985: MGPN SMC N = 1,13) and Morgan (1995: [$M95$] N = 1,9).

Our spectra were taken during different observing runs from 1984 to 1999 with various telescopes and instruments in ESO La Silla: the 1.52 m, 2.2 m, 3.60 m and NTT telescopes, and the B&C, EFOSC, EMMI spectrographs. The spectral range was always split into two regions, blue and red, with an overlap including at least the H_β – [OIII] lines. This choice was made to ensure an adequate spectral resolution (about 3–4 Å/pixel) and yet provide adequate spectral coverage. All spectra were reduced using MIDAS and its LONG package, following a standard procedure for 2D spectra, with optimized spectrum extraction and line fitting to measure the line intensities. Details of the observing and data reduction procedures can be found in Paper I (Sects. 2 and 3).

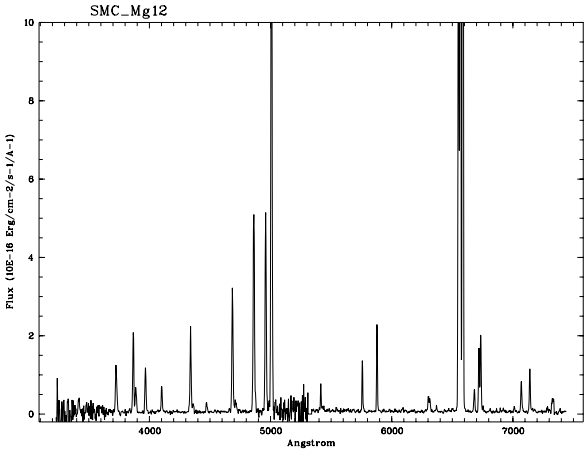

Fig. 1. An example of a type I PN in the SMC (MGPN SMC 12) with strong [NII] lines.

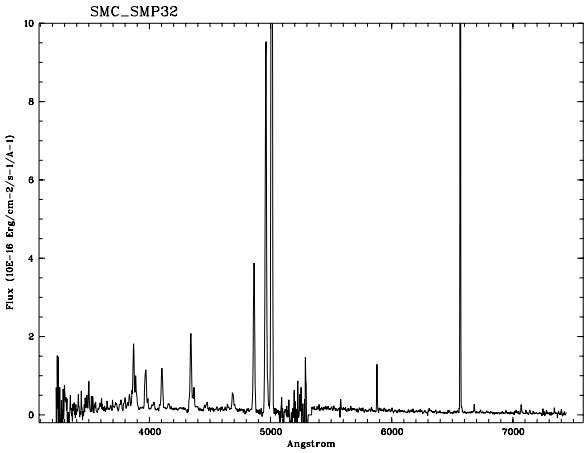

Fig. 2. A standard faint PN in the SMC (SMP SMC 32). Note the absence of [NII] lines.

To our own observations we added data for other objects taken from the literature, namely Monk et al. 1988 (hereafter MBC), Meatheringham & Dopita (1991a,b, hereafter MD), and Vassiliadis et al. (1992). We used corrected line fluxes from those lists (taking fluxes corrected for extinction as determined in the original paper) and then determined new abundances with our code, to obtain a homogeneous set of determinations. The total sample is thus composed of 65 objects observed by us, to which we add 118 other objects (not in common) with published line intensities.

To illustrate the high quality of our spectra, we show some examples in Figs. 1–5, of the PNe of various types in both Clouds. The blue and the red spectral ranges were observed separately, but merged in the illustrations. The S/N can be judged, for instance, from the strength of the [OIII] λ_{4363} line, a key line for temperature determinations.

As discussed in more detail in Sect. 4, a first analysis of the results showed some discrepant points in the diagrams, some of which could clearly be ascribed to poor quality spectra for some objects from the literature. We thus removed from the initial sample of 183 objects 8 PNe in the SMC and 18 in the LMC, where no [OIII] temperature determination was possible, and no

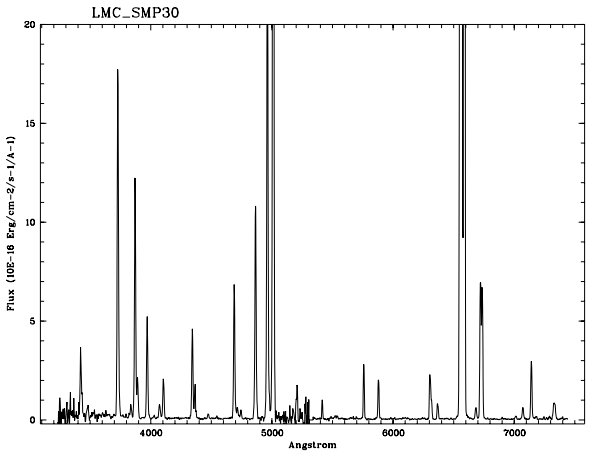

Fig. 3. A bright type I PN in the LMC (SMP LMC 30) with many emission lines observed, including [NeV] in the near UV.

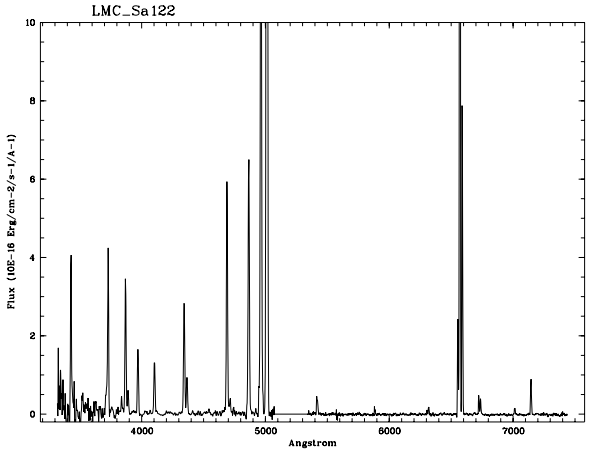

Fig. 4. A type i PN in the LMC (SMP LMC 122) (strong [NII] but very weak He I lines).

lines fainter than 10% of H_β were detected. This leaves us with a sample of 157 objects for the full analysis.

2.1. Comparison of line intensities

We have 30 objects from our observed sample in common with MD and 28 with MBC, thus providing a possibility for consistency checks. In Fig. 6 we present the comparison of the line intensities for the 19 LMC and 11 SMC objects in common with Meatheringham & Dopita (1991a,b).

At high intensities, the agreement is generally good, with differences smaller than 20–30%. Most of the discrepancies come from the $[OII]_{3727}$ Å lines or from lines that are at the edge of the observed wavelength domain (as in Meatheringham & Dopita 1991a, for instance), a difference that can most probably be ascribed to an imperfect extinction or to spectral response correction. If we examine Fig. 7 in the low intensity line region, i.e. the intensities smaller than $H_\beta \simeq 100$, we see larger discrepancies. In particular MD always find higher intensities than we do for the faintest lines. This is a general trend that can probably be explained by a lower S/N and poor determination of the continuum level.

We do not discuss the comparison in detail between our intensities and those of Monk et al. (1988) (28 objects in common) or Vassiliadis et al. (1992) (11 objects in common), as the quality of their data seems to be rather poor, as judged from the huge uncertainty/errors for those faint objects, and many of them have finally been rejected from the final analysis diagrams.

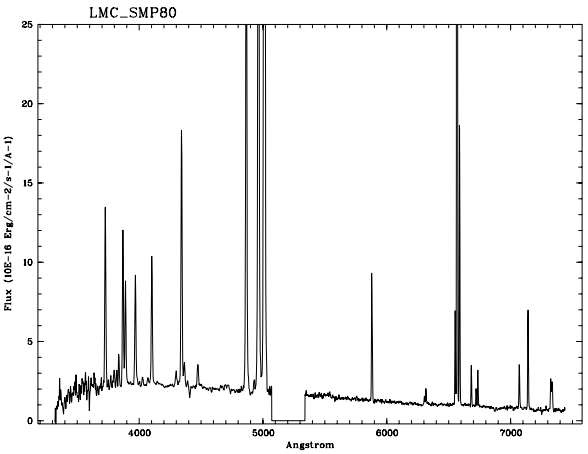

Fig. 5. A standard PN in the LMC (SMP LMC 80). The gap between the blue and red spectra is produced by the dichroic in the EMMI spectrograph at the NTT, used to record both wavelength ranges simultaneously.

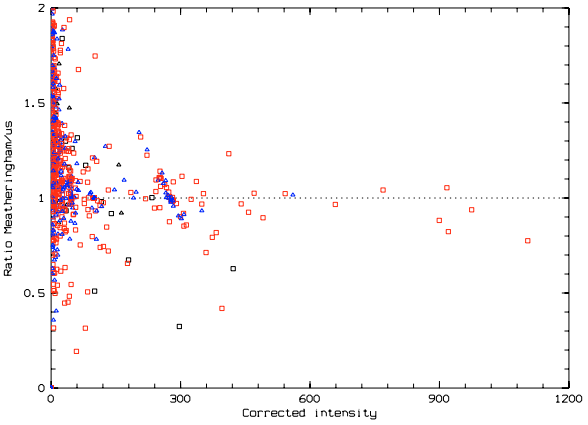

Fig. 6. Ratio of line intensities in the two independent observations, for the 21 PNe in common between us and Meatheringham & Dopita (1991a,b).

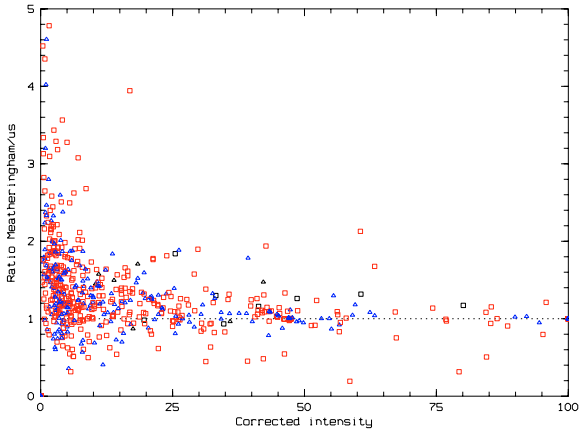

Fig. 7. Zoom of the previous figure (Fig. 6) at low intensities.

3. Physical parameters

3.1. Extinction

The Whitford (1958) galactic extinction law (noted $f(\lambda)$) was used in the parameterized form of Miller & Matthews (1972) for the optical domain. The uncertainties and differences between this galactic law and specific laws for the Clouds (e.g. Nandy et al. 1981) are such that this choice does not have a significant impact on the results in the optical range (contrary to the situation in Paper I, which included UV). The Balmer theoretical ratios were then used with (Eq. (1)) to determine the extinction coefficient $c(H_\beta)$ in an iterative way, two iterations being necessary because densities n_{e^-} and temperatures T_{e^-}, which affect the expected ratios, were calculated at the same time:

$$I_{cor}(\lambda)/I_{cor}(H_\beta) = I_{obs}(\lambda)/I_{obs}(H_\beta)10^{C(H_\beta)f(\lambda)}. \quad (1)$$

Three ratios, H_α/H_β, H_γ/H_β, and H_δ/H_β, were used to determine the extinction coefficient. When the three ratios gave very discrepant values, generally because of a low S/N ratio in the fainter lines, only the H_α/H_β ratio was used (see Paper I, Sect. 4.1 for more details). In the very few cases where we obtained a non-physical negative value for $c(H_\beta)$, the extinction coefficient was then set to zero.

The observed and corrected line intensities, $I_{obs}(\lambda)$ and $I_{cor}(\lambda)$, relative to $H_\beta = 100$, are given for all the objects in Appendix A. The corresponding H_β fluxes from the literature (Meatheringham et al. 1988) are also given in 10^{-16} erg cm^{-2} s^{-1} units, not corrected for extinction.

3.2. Temperature and density

The plasma diagnostics and the ion abundances were derived by solving the five-level statistical equilibrium equations with a code kindly made available by G. Stasinska and modified by us to update some coefficients or add more lines.

If possible we always calculated temperatures and densities from our code. The rules adopted for the final choice of temperatures are the following:

- if no $T_{[NII]}$ determination is available, then we take $T_{[NII]} = T_{[OIII]}$ if $T_{[OIII]}$ is in the 8000–30 000 K range; otherwise 12 000 K is adopted;
- if $T_{[OIII]}$ is not determined, but $T_{[NII]}$ is available; so we adopt $T_{[OIII]} = T_{[NII]}$, if $T_{[NII]}$ is in the 8000–30 000 K range (otherwise, 12 000 K is adopted arbitrarily);
- if no temperature determination is available at all, an arbitrary value of 12 000 K is adopted.

We compare the two temperatures ($T_{[OIII]}$ and $T_{[NII]}$) in Fig. 8. The alignment of points along the slope 1 line is due to the adopted rule $T_{[NII]} = T_{[OIII]}$, as a first approximation, when one of these temperatures could not be determined directly. Generally, however, both observations and models give $T_{[NII]}$ less than $T_{[OIII]}$ (as seen in the same figure). A better approximation has been proposed for Galactic objects by Kingsburgh & Barlow (1994) but is not directly applicable here, because the range of T and n_{e^-} encountered is much larger, and furthermore, such a relation is certainly very metallicity dependent. The figure shows that it seems to be a good approximation for some of the objects where both temperatures are determined but that it generally underestimates $T_{[NII]}$.

For electron density (n_{e^-}) determinations, the rules adopted are the following. We first derive the densities from [SII] lines (if available, and if the density is less than 50 000 e$^-$ cm^{-3}); otherwise, the density is derived from the [ArIV] lines, when available. If neither of these determinations is possible, we adopt a density of 5000 e$^-$ cm^{-3} (a value generally adopted in other published data). More details of the treatment can again be found in Paper I, Sect. 4.2.

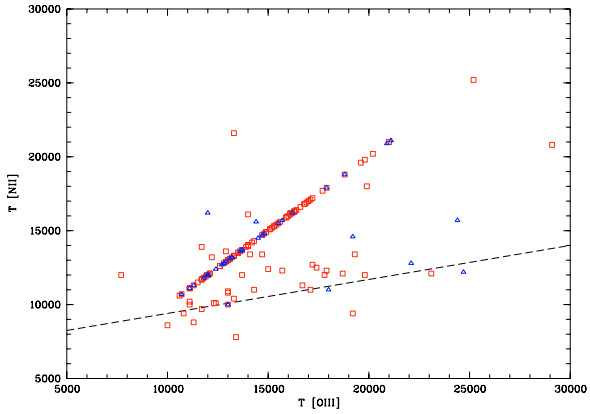

Fig. 8. $T_{[NII]}$ versus the $T_{[OIII]}$ temperatures. The relation found by Kingsburgh & Barlow (1994) for Galactic objects is plotted as a dashed line.

3.3. Chemical abundances-ionization correction factors

Ionic abundances were calculated relative to hydrogen from the recombination lines of He or from the forbidden lines of heavier elements. Total elemental abundances were then derived through ionization correction factors (ICF) to take the unobserved ionic stages into account. The details of the procedure and the ICF used are described in Paper I. The only change introduced in this paper is the use of a more accurate ICF for argon (Eqs. (2) and (3)), derived from models by Ratag & Pottasch (1990) and based on excitation class (EC) and observed ionic stages of the object.

When the [Ar III] and [Ar IV] lines are available, the ICF is:

$$\begin{aligned} ICF &= 1.39 \qquad EC < 4.5 \\ ICF &= 1.43 \qquad 4.5 < EC < 7.5 \\ ICF &= 1.75 \qquad EC > 7.5 \end{aligned}$$

$$\frac{N(Ar)}{N(H)} = \frac{N(Ar^{2+}) + N(Ar^{3+})}{N(H^+)} * ICF(Ar). \quad (2)$$

When only the [Ar III] line is observed, then:

$$\begin{aligned} ICF &= 1.73 \qquad EC < 4.5 \\ ICF &= 2.04 \qquad 4.5 < EC < 7.5 \\ ICF &= 3.85 \qquad EC > 7.5 \end{aligned}$$

$$\frac{N(Ar)}{N(H)} = \frac{N(Ar^{2+})}{N(H^+)} * ICF(Ar). \quad (3)$$

The excitation classes are derived analytically with the equations of Dopita & Meatheringham (1990).

3.4. Uncertainties

The final uncertainty on a given line depends primarily on its strength and on the quality (S/N) of the spectrum. The continuum noise level is a good indicator, but uncertainties in fitting the lines are also taken into account. The Hβ flux uncertainties

Table 1. Abundance differences between us and Meatherigham et al. (1988). The first line gives the mean difference averaged over several objects (the difference can be higher for an individual one), the second line gives the number of objects used in the determination, while the σ is given in the third line.

	LMC							SMC						
	He	N	O	Ne	S	Ar	N/O	He	N	O	Ne	S	Ar	N/O
Δ	–0.04	0.35	–0.01	–0.10	0.53	0.00	0.36	–0.06	0.49	–0.10	–0.23	0.67	0.00	0.58
Number	(36)	(36)	(37)	(36)	(32)	(0)	(36)	(6)	(6)	(6)	(6)	(4)	(0)	(6)
σ	0.08	0.32	0.18	0.23	0.61	0.00	0.31	0.06	0.30	0.14	0.23	0.41	0.00	0.24

Table 2. Same as Table 1 but for Monk et al. (1988).

	LMC							SMC						
	He	N	O	Ne	S	Ar	N/O	He	N	O	Ne	S	Ar	N/O
Δ	0.00	–0.18	–0.11	0.01	0.00	0.00	–0.06	0.03	0.01	–0.15	–0.12	0.00	0.00	0.17
Number	(6)	(6)	(6)	(5)	(0)	(0)	(6)	(4)	(3)	(4)	(4)	(0)	(0)	(3)
σ	0.05	0.14	0.17	0.03	0.00	0.00	0.18	0.06	0.06	0.08	0.12	0.00	0.00	0.10

given in Appendix A are a good representation of the quality of the spectrum.

For lines with intensities down to about 1% of Hβ (5% for very faint objects), the uncertainty scales approximately with the inverse square root of their intensity ratio to Hβ. For very faint lines (fainter than the above limit), the S/N gets worse, and the uncertainty scales approximately with the inverse of their intensity ratio to Hβ. As expected, for fairly bright objects, the majority of the spectra have very good S/N ratios, so they are among the best spectra available in the whole sample. For the faintest objects, sometimes only a few bright lines are well observed, and the quality of the results scales accordingly. An estimate of the uncertainty in the extinction coefficient, $c(\mathrm{H}_\beta)$, is also given, derived from the comparison of individual values obtained from each of the individual Balmer line ratios used in the determination. In addition to "absolute" uncertainties discussed above, comparing abundances derived by various authors for objects in common provides another way to derive the final uncertainty of abundances.

When comparing abundances derived from various observations of the same object, but all derived with our method, we find small differences of about ±0.05–0.10 for helium, carbon, nitrogen, and oxygen. In some cases, especially in the SMC, the difference for nitrogen can be about 4–5 times larger, which is probably due largely to the use of a high nitrogen temperature, following the set of $T_{[\mathrm{NII}]} = T_{[\mathrm{OIII}]}$. This question will be analyzed in more detail in a forthcoming paper where we intend to compare results from detailed photo-ionization models with those of ICF's for the objects with the highest S/N spectra. For neon and argon, the differences are ±0.10–0.20 and reach ±0.50 for sulfur.

We summarize in Tables 1 and 2 the differences between the abundance determinations for various elements in the Magellanic Clouds. The differences represent mainly the uncertainties in the observations, but one should note that the uncertainties on intensities published in the literature appear to be larger in general than those of our own observations.

If we now compare published abundances and our own determinations with the same intensities as input, we sometimes find large differences. This reflects the uncertainties due to, mainly, atomic data, the ICF, or the photo-ionization models. The agreement with MBC is usually excellent, as expected because we both use the same technique (ICF corrections).

The differences with MD are larger, reflecting the discrepancies between modeling and ICF methods. We therefore find the usual differences here between ICF and model determinations.

The abundance differences of oxygen or neon are acceptable (0.10–0.15), but they are definitively too large for helium or nitrogen. MD always finds a greater He abundance by about 0.05 dex (Table 1). This difference becomes smaller (about 0.05 dex) if we use only the He I λ_{5876} line. Uncertainty on the faint λ_{4471} and λ_{6678} He I lines could be one reason, but inaccuracies in the instrumental response curves is another factor that is not easy to estimate. For a few individual objects, large abundance differences found between various authors result from a markedly different temperature and/or density determination. Such cases will be discussed individually later.

We can summarize our own abundance determination uncertainties as follows:

- 0.05 dex or less for He;
- about 0.10 dex for C, O and Ne;
- about 0.15–0.20 dex for N (because of larger ICF) and Ar;
- up to ~0.4–0.5 for S.

Ratios, such as the N/O one, are of course much less sensitive to temperatures or ICF errors and have been used whenever possible in the following.

4. Results

In the following, we discuss the various abundances patterns in detail.

4.1. Tables

The physical parameters, $c(\mathrm{H}_\beta)$, n_{e^-}, $T_{[\mathrm{OIII}]}$, $T_{[\mathrm{NII}]}$, excitation class, and total abundances for all the studied objects are presented in Tables 3 and 4. Mean abundances in the ISM of both Clouds, for reference, are taken from H II regions, as compiled by Dennefeld (1989). Another compilation by Garnett et al. (1999) gives values in excellent agreement (within 0.05 dex).

The mean values for H II regions are shown in the figures. Solar values are from Grevesse & Anders (1989). Note that adopting the recent, lower, solar value proposed by Allende Prieto (2001) instead would not affect our discussion, as all comparisons are made with respect to the H II regions values. Objects intermediate between "normal" PNe and "classical" type I's in the standard definition, which we called type i in

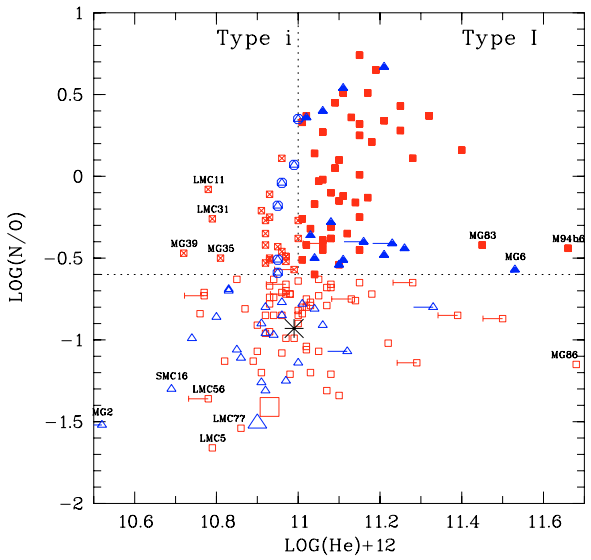

Fig. 9. N/O-He/H. Squares are for LMC objects and triangles for SMC ones. Filled symbols represent type I PNe, and open symbols "standard" PNe. The type i's (see text) are represented by crossed squares (LMC) or circled triangles (SMC). The star marks the solar value. The same symbols will be used in all subsequent figures. The vertical and horizontal dotted lines indicate the separation between type I, type i, and "standard" PNe. In all the figures, LMC objects are plotted in red squares and SMC ones in blue triangles, the color figures being available in the electronic form of this paper.

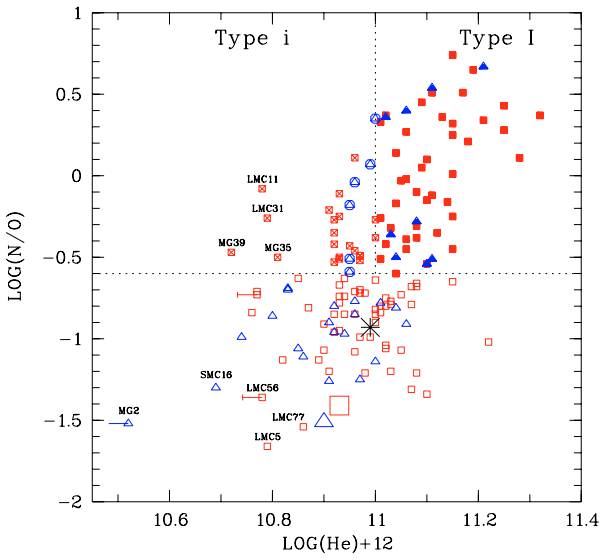

Fig. 10. N/O-He/H. Same as Fig. 9, but only with objects with accurate determinations (see text Sect. 4.1).

Paper I, and defined as those objects having an excess in N/O but not in He.

In Table 5 we note the presence of some peculiar emission lines, identified in a few objects of our sample (and also seen in WR stars). The observed intensities are given in the same units as before (H_β = 100). The symbol ~ indicates only a marginal detection. In the literature, only 5 objects are classified as Wolf Rayet objects:

- SMP SMC 6 and MGPN SMC 8;
- SMP LMC 38, SMP LMC 58 and SMP LMC 61.

We point out in Table 6 some objects that we observed in H_α imaging, and that appear to be resolved. Some comments on their morphology are given also.

Although we should now discuss the various abundance patterns, but in any diagram, such as for instance the first one where we compare N/O to He/H (Fig. 9) for the 183 objects, objects lying outside the average location of the PNe call attention to themselves. Such "outliers" could be very interesting in having extremely high (or low) abundances compared to the average value, provided we are certain this abundance determination is not affected by larger-than-average uncertainties (due to a poor quality spectrum, or a poor temperature determination, etc). We therefore checked all those objects one by one. In some cases, the spectra are of poor quality with only a few bright lines available, and they account for the upper limits in He seen in Fig. 9 and will be removed from further analysis. In total, 27 objects were eliminated due to poor quality spectra, eight in the SMC and nineteen in the LMC.

Note also that for 8 additional objects with better spectra, the temperature and or density could not be derived directly from line ratios, so that an arbitrary value had to be assigned. This is provisionally adequate as the range of densities and temperatures in PNe is usually limited, but these objects deserve special care in the discussion. There are 5 in the LMC: SMP LMC 64, SMP LMC 94, MGPN LMC 35, MGPN LMC 39, and [M94b] 50; and 3 in the SMC: MGPN SMC 2, MGPN SMC 8, and LHA 115-N 8.

The removed objects are essentially from the data of Vassiliadis et al. (1992): all of them deserve further observations, and will be studied again in the future. The N/O versus He/H diagram is then redrawn in Fig. 10 with the remaining 156 objects which will be the basis of further analysis. Remaining outliers (which cannot be ascribed a priori to a poor spectrum or a poor temperature/density determination) will be discussed when they appear in the following figures (Figs. 10–23), but all are collected together in Table 7.

4.2. Helium and nitrogen

As already discussed in our first paper, the type I PNe were introduced by Peimbert (1978, 1984) for Galactic objects, because they could be clearly separated from other PNe in an N/O versus He/H diagram. We present such a diagram in Fig. 10, now with a large sample according to the original definition, but corrected for the different metallicity in the LMC or SMC, as discussed in Paper I. There is a smooth continuity between the two types,so that it now becomes difficult to separate the PNe in these 2 different classes from observational data alone (although the distinction is clear on theoretical grounds). Because of the addition of many faint nebulae, the dispersion of the points has also increased. Type i objects, introduced in Paper I, appear in the upper left part of the diagram (following their definition: high N/O but not high He). Here also, the separation between type I and type i is now arbitrary, as both classes, with high N/O, cover a continuum in He abundances. Clearly the original abundances (at the time of the formation of the progenitor) need to be known in order to distinguish the various objects by their level of enrichment.

The N/O ratio increases with He/H, however the slope of the correlation is different for the 2 classes. This correlation is interpreted as due to the mixing of the 2nd *dredge-up* products (He and N) into the envelope. The type i PNe seem to prolong the type I PNe correlation, (characterized by a larger helium enrichment, in Fig. 9), rather than the relation for the

Table 7. Outstanding objects in various diagrams. For each of them, we give in the first line its name, the adopted temperature and density, and the elemental abundances that seem to be abnormal. The second line gives the ICF used in the corresponding column, so that a check can be made of whether the problem comes from there or from another source. A ∗ symbol in front of the density or the temperature indicates that this value could not be derived directly from line ratios (see Sect. 3.2).

Name	Ne-	T_{OIII}	T_{NII}	N/O-He	He-Ar	N/O-N	N/O-O	N/O-Ar	Ne-O	O-Ar
SMP SMC 1	*5000	11 000	11 000						6.42, 7.86	
									1.22, 1.01	
SMP SMC 16	*5000	11 800	11 800	−1.30, 10.69					6.37, 7.85	
				2.04/1.02					2.02, 1.02	
SMP SMC 32	5000	14 700	14 700					−0.91, 4.83		7.95, 4.83
								134/1.14–1.14		1.14–1.73
MGPN SMC 2	*5000	*12 000	*12 000	−1.52 < 10.52	10.52, 6.00					
					1.73					
MGPN SMC 12	1300	22 100	12 800	0.67, 11.21			0.67, 7.47		7.10, 7.47	
				5.24/1.62			1.62		2.34, 1.62	
SMP LMC 11	6200	29 100	20 800	−0.08, 10.78		−0.08, 7.10	−0.08, 7.18	−0.08, 4.99		
				3.07/1.30		3.07	1.30	3.07/1.30–2.04		
SMP LMC 26	*5000	13 600	13 600	−0.13, 09.85		−0.13, 6.93	−0.13, 7.06		6.90,7.06	
				1.00/1.00		1.00	1.00		1.00–1.00	
SMP LMC 31	6600	14 000	16 100						5.58, 7.29	
									1.92–1.02	
SMP LMC 54	400	11 700	11 700		11.10, 6.63			0.11.6.63		
					3.85			2.96/2.09–3.85		
SMP LMC 55	47 400	12 200	9600						6.80, 8.40	
									9.00–1.01	
SMP LMC 56	*5000	13 100	13 100	−1.36, 10.79						
				2.48/1.14						
SMP LMC 64†	*5000	*12 000	*12 000	−0.71, 10.76			−0.71, 7.05			7.05, 5.66
				1.80/1.01			1.01			1.01–1.73
SMP LMC 99	3600	12 200	12 200		10.92, 6.62			−0.41, 6.62		
					1.43			20.2/1.32–1.43		
MGPN LMC 39	*5000	25 100	25 100	−0.48, 10.72						
				2.60/1.07						
[*M*94*b*] 8	10 600	16 800	16 800						<5.91, 7.66	
									2.71–1.03	

† Dopita & Meatheringham (1991b) have dedicated a paper to study of this peculiar high density object.

non-type I PNe. On the other hand, it appears that many of them have low initial abundances, as can be seen in a He versus Ar diagram. To show once more that we believe this is a real effect and not due to poor abundance determination, we present this diagram in the two forms again: with the full initial sample in Fig. 11 and after removal of the poorly determined objects in Fig. 12 (from here onwards, we will then always be only working on the clean sample of 157 objects). To conclude then for the type i PNe, the four objects with lowest He abundance, but N/O above −0.6 (our definition of type i), SMP LMC 11, SMP LMC 31, MGPN LMC 39, and MGPN LMC 35, also have a low argon abundance (Figs. 12, 16). The first three also have a low oxygen and a low neon abundance (Fig. 21). This may therefore indicate that the major difference between type I's and type i's lies in the lower initial abundances for the latter.

We now discuss the global properties of the N/O versus He/H diagram (Fig. 10). Note that two objects with very low He abundances, SMP LMC 26 and LHA 120-N 99 (Monk et al. 1988), lie outside the diagram, but are very low excitation objects for which a good He abundance determination is difficult. A few objects have both low He and low N/O: for instance SMP SMC 16, SMP LMC 5, SMP LMC 56, SMP LMC 77. As they also show a low Ar (or O) abundance, these are also candidates for progenitors with low initial abundances (and therefore older). However, SMP LMC 77 also has a high carbon abundance (unfortunately the only object in this group with a known C abundance) and can therefore be an object where the processing has gone further than the triple-alpha reaction and destruction of He, favored by a low initial abundance (as discussed in Paper I). All those objects should therefore also be observed in the UV to determine their carbon abundance.

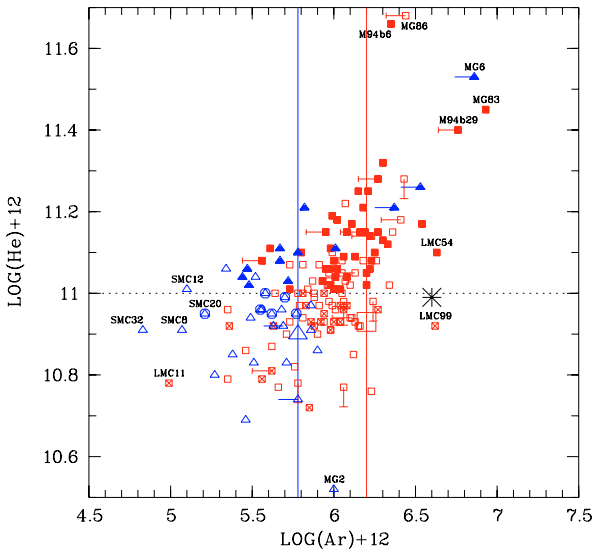

Fig. 11. He/H versus Ar/H. The vertical lines are marking the average HII regions values in argon for SMC and LMC. Symbols as in Fig. 9.

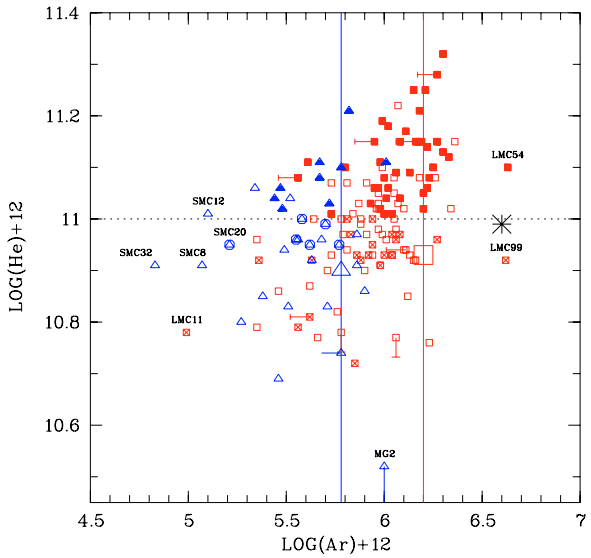

Fig. 12. He/H-Ar/H, as Fig. 11, but only with objects with accurate abundance determinations.

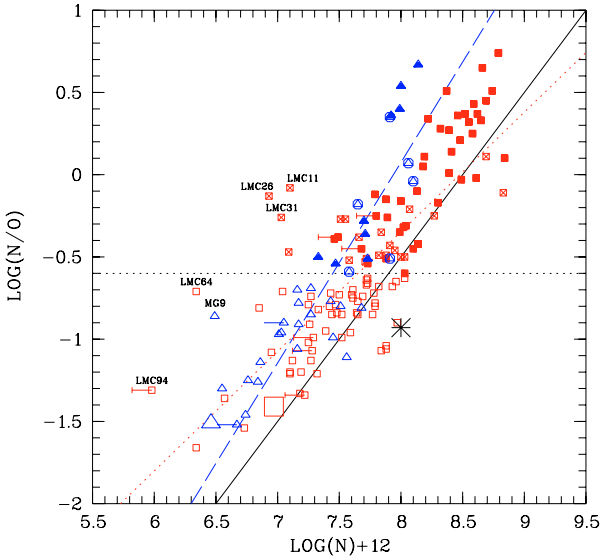

Fig. 13. N/O-N/H relation. Symbols as in Fig. 9. The dotted line is the fit to LMC objects, and the dashed line the fit to SMC objects. The continuous line is the relation for Galactic objects as shown by Jacoby & Ciardullo (1999).

A correlation between N/O and N/H is seen in Fig. 13. The large sample available here allows us to distinguish different slopes for the two Clouds (N/O = $a \times$ (N/H) + b):

- for LMC, $a \simeq 0.727 \pm 0.047$;
- for SMC, $a \simeq 1.220 \pm 0.039$.

These different slopes are an indication that the enrichment processes are more efficient in metal poor galaxies, as already suggested in Paper I.

The "peculiar" objects in this diagram are the same ones already discussed in Fig. 10, with the addition of three more with low N abundance: MGPN SMC 9, SMP LMC 64, SMP LMC 94. SMP LMC 64 is a peculiar object with extremely high densities and temperature, already discussed by Dopita et al. (1991b). MGPN SMC 9 and SMP LMC 94 both seem to be low in abundances for many elements and are therefore candidates with an old progenitor.

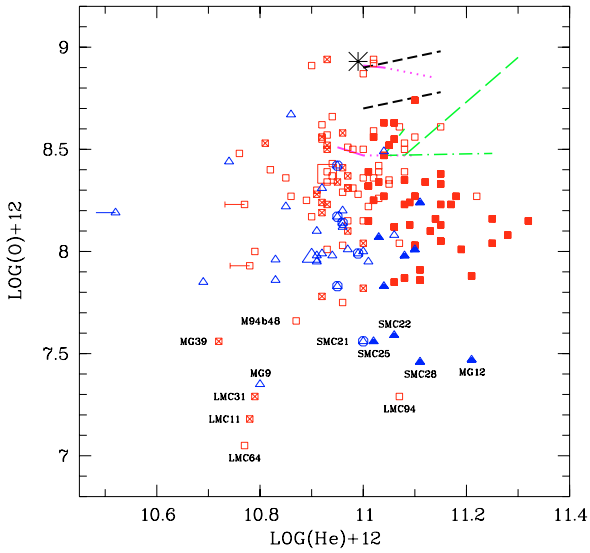

Fig. 14. Relation between oxygen and helium abundances. The various line segments are the predictions from the models of Marigo et al. (2003). Upper curves are with galactic metallicities, and lower with the LMC.

4.3. Oxygen

In studies of the chemical evolution of galaxies through the analysis of gaseous nebulae, the oxygen abundance is usually taken as a reference for the global metallicity and then used as the tracer of the evolution. When starting this project, it was our intention to follow this practice and use the oxygen abundance, as measured in PNe, to characterize the metallicity of the galaxy at the time when the PN progenitor was formed. While the lifetime of the nebula and its progenitor star is relatively short for H II regions compared to the total lifetime of the galaxy, and hence oxygen there measures the metallicity at the present time (at least locally) for PNe, this method assumes, however, that no processing of the initial O abundance has occurred during the life time of the progenitor star. It rapidly became clear (see Paper I) that this usual assumption should be questioned, especially for low metallicity galaxies: the oxygen abundance measured in PNe does not seem to be very different from the mean abundance in H II regions, although some progenitors might be rather old. Looking in more detail at the various diagrams, we see that about half of the PNe (and more for the SMC than for the LMC) have oxygen abundances even above this average value, some of them with large over-abundances (see for instance Fig. 14). This fact is already present in earlier data by various authors, but was never specifically commented on. The large sample available here allows a detailed discussion of this problem.

The enrichments in PNe are much more apparent in the Magellanic Clouds than in our Galaxy, which is clear for nitrogen or carbon, but also seems to be the case for oxygen. On average, it appears that the enrichment in oxygen could be as large as the amount present at the time the progenitor star was formed. Therefore the question of oxygen production cannot be neglected anymore. On the other hand, a fair fraction of PNe have lower oxygen abundances than the average H II value, but it is not clear whether this reflects the initial abundance directly, or whether it also includes some destruction during the AGB phases.

Indeed, oxygen abundances can be affected by processing in the PNe progenitor stellar cores, in at least two ways. On one hand, oxygen destruction can occur during the CNO cycle

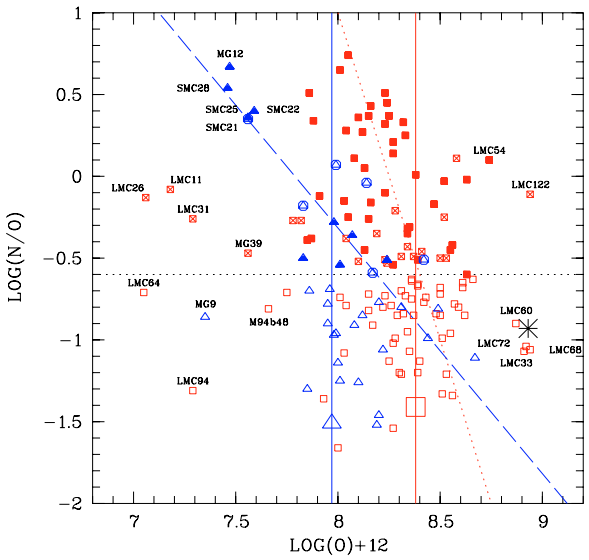

Fig. 15. N/O-O/H relation. Symbols as in Fig. 9. The dotted (LMC) and dashed (SMC) lines are only fits to the type I nebulae. The vertical lines underline the HII regions mean abundance values, while the horizontal one marks the separation between type I and "standard" nebulae.

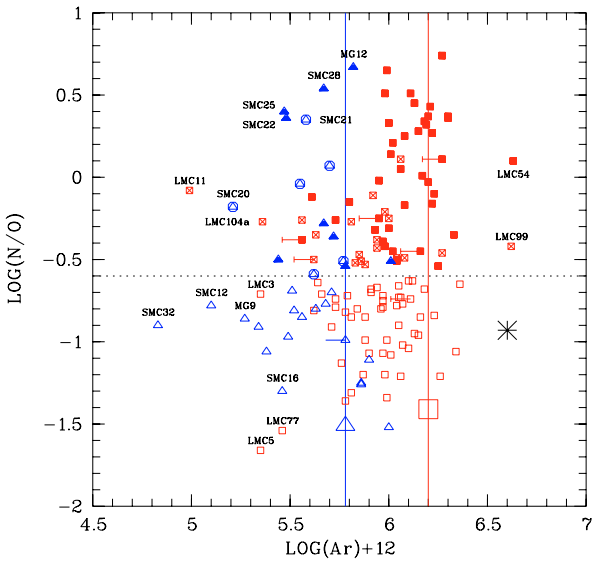

Fig. 16. N/O-Ar/H relation. Lines as in Fig. 15.

in the more massive progenitors (specifically the ON cycle) and thus affects the abundance seen in the nebula. On the other hand, nebular abundances, in particular carbon, could be substantially modified during the 3rd dredge-up by mixing with freshly core-processed material (Paper I). This mixing could also lead to enhancement of the oxygen abundance. In the next two sections, we look for evidence of such modifications which, if demonstrated, will require the definition of another metallicity tracer, unaffected by processing during the life-time of PNe progenitor stars.

4.3.1. Oxygen destruction

Figure 15 presents the N/O versus O relation. It appears that about half the SMC type I nebulae display lower oxygen abundance than average, lower than the mean value given by the HII regions. This effect is also present for the LMC objects, but partly hidden by some outliers with higher O abundance, which will be discussed at the end of this section (the objects with both low O *and* low N/O are the same ones as were already singled out in the previous diagrams). The overall effect is best seen when introducing the slopes of the relations for type I objects only (Fig. 15). The type i objects are more dispersed, and will be discussed specifically later.

As the type I nebulae are generally believed to arise from higher mass and therefore younger progenitors (Peimbert 1985; see also Stanghellini et al. 2000), this effect cannot be due to a lower initial metallicity. This is indeed demonstrated in Fig. 16 where Ar is plotted instead of oxygen in abscissa: the type I nebulae are the ones with the largest argon abundance, which is typical of younger objects. It is significant that essentially no reliable object has, within the error bars, a larger argon abundance than in H II regions, contrary to oxygen (see Sect. 4.4). The two noticeable exceptions are SMP LMC 54 and SMP LMC 99). The simplest explanation is that we observe some oxygen destruction, as predicted by stellar evolution models, especially for the higher masses where the ON cycle should be more efficient.

The observed trend is metallicity dependent, because it is not seen in our Galaxy and is small in the LMC and much greater in the SMC, therefore implying a metallicity dependence for the corresponding nuclear reactions. This dependence, and the large sample of objects used here, indeed helps to emphasize this effect. As a consequence of this oxygen depletion, the N/O enhancement is therefore even larger than previously thought in type I nebulae (see also Fig. 17, O/H versus Ar/H).

An anti-correlation between N/O and O is also apparent in Fig. 15, and is more pronounced for SMC objects than for LMC ones. This anti-correlation has been known for quite some time (Peimbert 1985) and has been discussed more recently, although with a much smaller sample of objects, by Costa et al. (2000). It is also interpreted as due to a higher efficiency of the surface enrichment through dredge-ups at lower metallicities. Costa et al. (2000) also argue that the effect is even clearer when PNe are grouped by mass range of their progenitor star, but we cannot do this here in view of the very few masses really known in the Clouds. A hint of this is seen in Fig. 15, as the anti-correlation is more pronounced in the upper part of the diagram (type I objects) than in the lower part populated by "standard", presumably less massive objects.

In a recent study of ten Galactic objects, Marigo et al. (2003), in discussing an O-He diagram, point out that high He abundance (He/H > 0.14 by number, that is log(He) = 11.15) is correlated with a low oxygen one. While this could be an obvious sign of the onset of the ON cycle in the most massive objects, they argue against this hypothesis, because their models then predict too high a nitrogen abundance, and prefer to assume a lower initial metallicity despite the problems raised by such low metallicity in objects close to the Galactic center. The same diagram for our objects can be seen in Fig. 14, with the results of Marigo's models superposed: the situation is more complex and the models do not reproduce all the observed data well. While objects with both low helium and low oxygen (as seen in the LMC, in particular) are probably objects with low initial metallicities, the LMC objects with the highest helium content, log (He) > 11.15, which are all type I's by definition, do indeed present a lower oxygen abundance than the average non-type I. This cannot all be ascribed to variations in initial composition, or else it would also be reflected in other elements, such as argon, which is not the case. We therefore need to invoke oxygen destruction via the ON cycle. This is entirely consistent, as the ON cycle is

believed to operate only in the most massive progenitors, i.e. those of type I nebulae. Some objects in Fig. 15 have a much higher oxygen abundance than the HII regions, such as SMP LMC 54 or SMP LMC 122 (a type i). This implies that we cannot exclude oxygen production, particularly for type I and type i objects. In those nebulae, the observed oxygen abundance is then the combined result of both destruction and production. These two examples probably have intermediate-mass progenitors (less than 3 $M_{\odot}$), where oxygen production should be possible.

4.3.2. Oxygen enrichment – CO core and thermal pulses

In Paper I we have shown that the carbon abundances are highly enhanced in the Magellanic Clouds. As discussed there, the 3rd dredge-up occurs in all PNe, but its efficiency appears to be higher with lower initial metallicities. The N/O versus O anti-correlation (discussed in the previous section) is interpreted the same way. This has also been shown by Costa et al. (2000) and theoretically confirmed by Marigo et al. (2003). This fact offers also an easy explanation for the higher number of carbon stars found in galaxies with metal-deficient composition. During the 3rd dredge-up, however, the carbon is not the only element transported. In the CO core, oxygen has been produced by α capture on a carbon nucleus $^{12}C(\alpha,\gamma)^{16}O$, although this process has a smaller probability of occurring than the 3α process. It is possible (as suggested by the oxygen abundances observed here, often higher than the ones of HII regions) that the nuclear reaction rate of this reaction is not as accurately known as previously thought (Bono 2000; or Metcalfe et al. 2002).

On the other hand, during the thermal pulses, the fusion of Hydrogen produces ^{13}C (and not ^{14}N) for central stars with core masses smaller than 1 $M_{\odot}$. Oxygen is then also produced from $^{13}C(\alpha,n)^{16}O$. This reaction is a strong source of neutrons, inducing the *s process*: the observed over-abundances of some high atomic weight elements in AGB stars is proof of its operation. It would thus also contribute to the production of oxygen.

A recent model with overshooting (Herwig 2000; Werner & Herwig 2005) determines layers where the chemical composition is even more enhanced in oxygen than in the standard CO core composition (by number):

- helium: 25–33% (instead of 22%);
- carbon: 50% (instead of 76%);
- oxygen: 17–25% (instead of 2%).

With such a core composition, the 3rd dredge-up in operation, and the strong helium and carbon enrichment observed (up to 100 times for C, or even more), one can expect an enrichment in oxygen, too. This would be particularly visible in the Magellanic Clouds, because the quantity of metals present in the progenitor star is initially low, and the enrichment processes are more efficient at lower metallicity.

This therefore seems the easiest explanation for the observed enhancement in oxygen. It may at the same time represent observational evidence for the existence of overshooting. When comparing the core composition in models with and without overshooting, it also appears that the carbon fraction is higher in the latter (the reverse is true for oxygen): a precise determination of C abundances in more PNe would therefore be a key observation confirming this interpretation. A simple evaluation can show that a reasonable number of thermal pulses (a few tens) are enough to produce the required quantity of oxygen to match the observed oxygen abundance and, at the same time, achieve the huge enrichment seen in carbon.

Recent semi-analytical models by Marigo et al. (1996) and Marigo (2001) agree closely with our observations, and with the possibility of oxygen production (within some initial mass range). While the oxygen production for an initial solar metallicity is negligible, enrichment is predicted at low metallicity (at $Z = 0.008$, as in the LMC). But with an LMC initial composition, the oxygen production in Marigo's models is only strong in the $1.5\ M_{\odot} < M < 3\ M_{\odot}$ mass range. This is consistent with type I PNe in the Magellanic Clouds with initial star masses greater than 3 $M_{\odot}$, as no clear oxygen enrichment is seen in them. It would be desirable to have such models calculated for even lower metallicities, such as SMC ones, to confirm the trend observed in our data. Charbonnel (2005) emphasizes that the surface abundance of ^{16}O in massive progenitors is the result of the competition between efficiencies of the third dredge-up (for production) and hot-bottom burning (for destruction), but that rotation also significantly enhances the surface abundance following the second dredge-up, especially at low metallicities. We can provisionally conclude that, as shown by the models, the explanation of the large observed enrichments lies both in the lower initial metallicities and in the corresponding increase in duration and efficiency of the phases of thermal pulses at the end of the AGB stage.

We note that the objects where oxygen production has probably been strong, such as those with much higher oxygen abundance than in the HII regions (as seen, for instance, in Fig. 17: SMP LMC 122, SMP LMC 33, SMP LMC 60, SMP LMC 68, or SMP LMC 72) are generally not type I objects. They stand out in Fig. 15 because of their low N/O (presumably due simply to their high O), but they do not show signs of peculiar N or He production, and should therefore have progenitors with lower masses where the HBB was not active. A carbon-abundance determination would be helpful for reaching a conclusion.

Globally, production of oxygen (for all masses) and destruction of it (for the higher masses only) compete for the net result; the enrichment appears to be maximal in an intermediate mass range (typically 1.5 to 3 $M_{\odot}$ for an LMC composition), but the net effect for higher masses is destruction of oxygen. When looking then at the type i objects, which are rather dispersed in oxygen abundance in Fig. 15, the consequence from the above is that the ones with higher oxygen abundances (SMP LMC 54 and SMP LMC 122, right side of the diagram) should have lower progenitor masses than the ones on the left side, such as SMP LMC 11 or SMP LMC 26, where oxygen destruction has been dominant.

4.4. Argon and sulfur

The only other elements whose abundances can be determined easily from optical spectroscopy are argon and sulfur. In spite of the weakness of the observed lines, argon is a good element for use in the determination of the initial composition of PNe central stars, so it should not be affected by transformations during the AGB phase.

Figure 17 shows that indeed only a few objects exhibit a larger argon abundance than in H II regions (contrary to oxygen). The points are grouped well around the line of slope 1 fitted to the H II regions and solar values. The average uncertainty on argon abundances should not exceed 0.2 dex by much, and the few points with values significantly above the H II regions all correspond to peculiar objects (SMP LMC 54 and SMP LMC 99), as already pointed out in previous diagrams. Furthermore, the type I PNe all have abundances close to the H II regions' mean value, confirming that these objects are

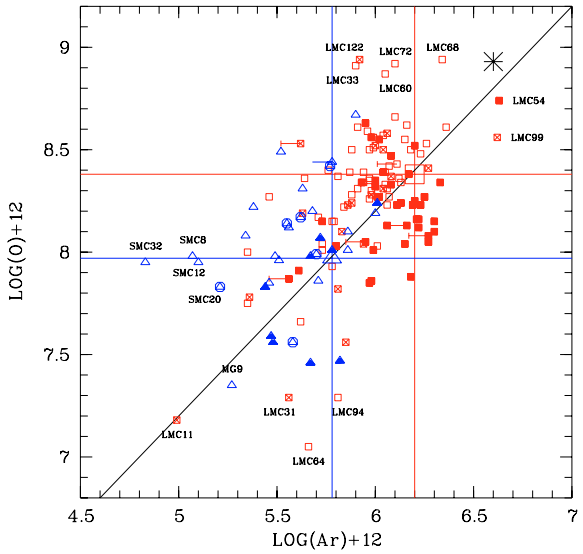

Fig. 17. O/H-Ar/H relation. The diagonal is the line with constant O/Ar going through the SMC and LMC HII regions values, which are underlined by the vertical and horizontal lines.

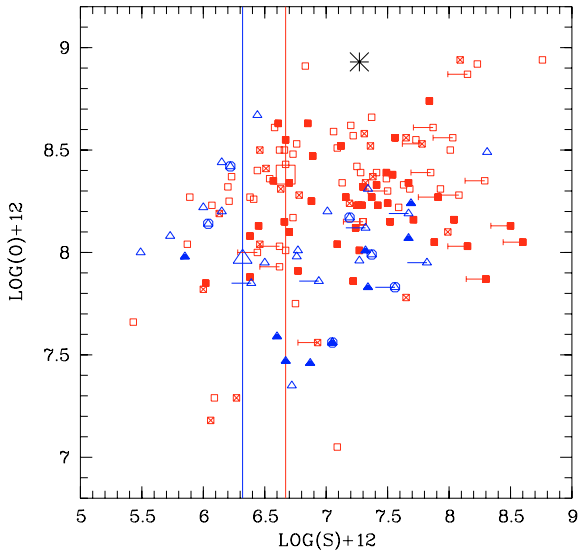

Fig. 18. O/H-S/H diagram with all the objects. Symbols and lines as in previous figures.

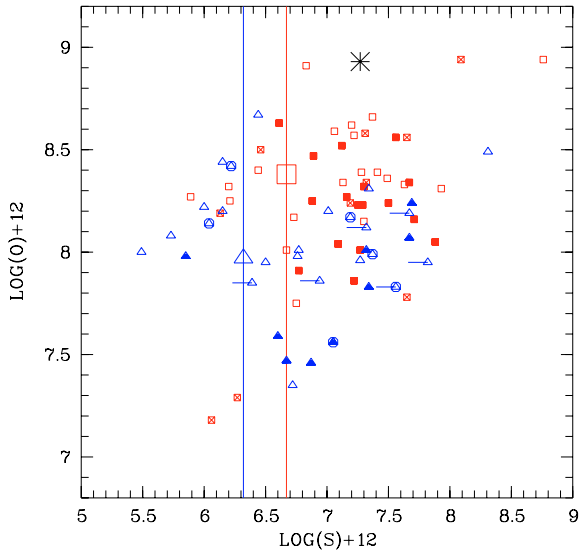

Fig. 19. O/H-S/H diagram as Fig. 18 with only the objects with best S determination (see text).

massive and young. Argon could therefore be used instead of oxygen as a good tracer of chemical evolution or time.

The same should be true for sulfur, at least from a nucleosynthesis point of view. In Fig. 18, a broad correlation appears between oxygen and sulfur, but with higher dispersion than for argon. Here many objects seem to have high abundances when compared to H II regions. This can, however, not be taken at face value, as the accuracy of sulfur abundance determinations is affected by well known problems. In particular, for high excitation objects like many PNe, the contribution of [SIV] lines to the abundance determination is essential (see, e.g., Dennefeld & Stasinska 1983) but is not available here. For many objects, we do not even have a detected [SIII] line. Adding the fact that the only available [SIII] line (in our observed range), the λ_{6312} Å line, is often too weak or blended with an oxygen ([*OI*]) line and that an electronic temperature in the sulfur zone should be derived as well for the ICF method, we end up with a rather large inaccuracy in the sulfur abundance determination. An effort is underway to improve this by complementary observations (Leisy & Dennefeld, in preparation). For the moment, we can try to improve the picture by taking only objects where both [SII] and [SIII] are available (as in Fig. 19). Then about only half of the PNe are usable, the dispersion in the sulfur diagrams is reduced, and most objects with large ICF also disappear. But the sulfur abundance determination is still not good enough to use sulfur as the metallicity indicator. One would for instance expect a good correlation between S and Ar, but Fig. 20, where a line of unit slope is plotted for reference, shows that the correlation is still not as good as expected, undoubtedly due to the poor sulfur abundance determination. Sulfur can therefore not yet be taken here as an element to replace oxygen as a tracer of the chemical evolution with time, although it is produced basically by the same progenitor stars as oxygen. This can be improved in the future by complementary observations in an extended spectral range.

4.5. The oxygen-neon relation

Figure 21 shows the Ne/H versus O/H diagram, where a good correlation can be seen between these two elements. The full line is a unit slope line going through the H II region points only, along which all the PNe points are well-grouped. A relation between O and Ne was already mentioned, e.g. in our Galaxy by Henry (1989), who interpreted it as a sign that these two elements were not significantly altered by nucleosynthesis in PNe. The relation is much better defined here in the Clouds alone, because of the larger number of objects available, but is however more difficult to understand now in view of the oxygen variations discussed in the previous sections.

The main correlation seen in Fig. 21 is not due to an ICF bias, because there is no obvious relationship between the (oxygen-dependent) ICF and the neon abundances, as can be seen from Fig. 22. Only one object with a high ICF, SMP LMC 55, falls off the main relation in Fig. 21, but its neon abundance is too low, not high.

The type I objects are slightly offset from the mean relation in Fig. 21, as already noted by Henry (1989), with a more pronounced difference at the low metallicity end. This offset

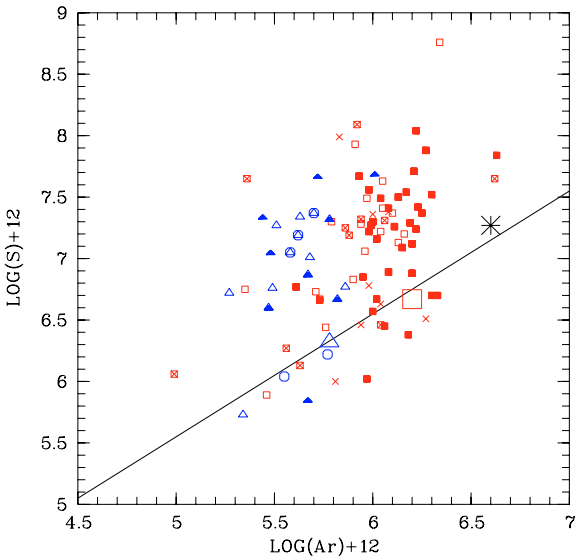

Fig. 20. S/H-Ar/H diagram with only the objects with best S determination. Objects with upper limits in both elements are not plotted. The continuous line is a slope 1 line going through the HII regions, for reference.

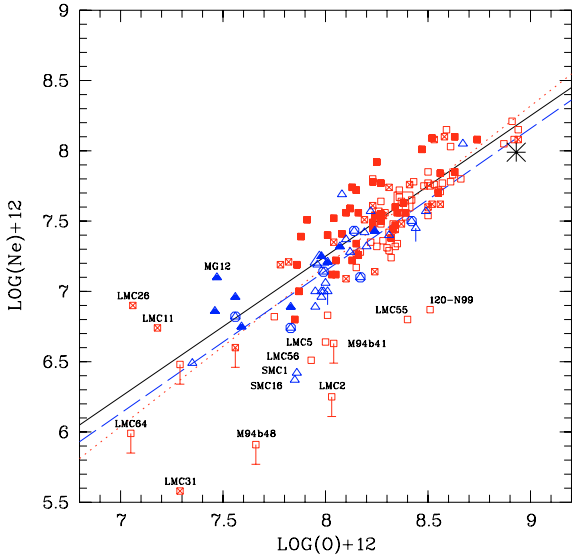

Fig. 21. Relation between neon and oxygen abundances. The dotted (slope 1.13) and dashed (slope 1.01) lines are the fit to the LMC and SMC objects, respectively, while the continuous one is a slope 1 line going through the HII region values.

can be understood as due to some oxygen destruction in the most massive objects with larger efficiency at lower metallicities, as discussed earlier. A clear example is the type I object MGPN SMC 12. The correlation seen in Fig. 21 implies that, if the oxygen abundance is enriched by some process, the neon abundance has to be enriched, too, to follow the correlation with oxygen. This is particularly true for those PNe with higher abundances than in H II regions. It can be understood with standard nuclear reactions such as $^{14}\mathrm{N}(\alpha,\gamma)^{18}\mathrm{O}(\alpha,\gamma)^{22}\mathrm{Ne}$ where the newly produced ^{14}N is almost completely converted into ^{22}Ne in a rich α environment. Neon could eventually be destroyed to produce Magnesium via the reaction $^{22}\mathrm{Ne}(\alpha,n)^{25}\mathrm{Mg}$, but this reaction has a very low efficiency (1%) unless the final core mass is greater than 1 $M_{\odot}$. As the majority of PNe central stars have core

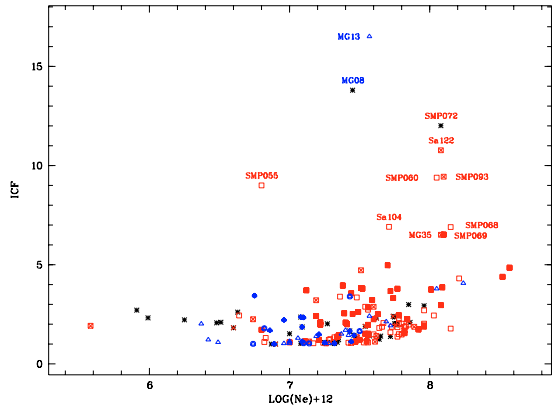

Fig. 22. Ionization correction factor (ICF) for neon. Symbols as in previous figures; stars indicate objects with poor determinations.

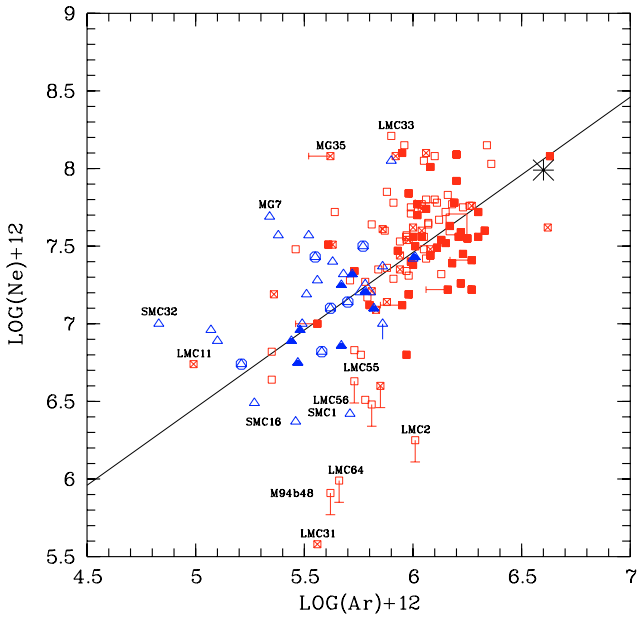

Fig. 23. Ne/H-Ar/H relation. The continuous line goes through the HII region values.

masses below this limit, the freshly produced neon should therefore not be destroyed, except in the most massive progenitors.

Alternately, the neon production could directly correlate with oxygen if the $^{16}\mathrm{O}(\alpha,\gamma)^{20}\mathrm{Ne}$ reaction were at work, but the reaction rates should then be higher than is actually believed. The fact that neon production is linked to oxygen is strengthened by the absence of correlation with other elements; e.g. in Fig. 23, the Ne-Ar relation displays a large dispersion where Ne varies over two and a half dex, while Ar varies over slightly more than one dex only. There is indeed no theoretical link between neon and argon productions, and argon is not expected to be produced or destroyed in PNe either. It also seems that the O-Ne relation is tighter for higher abundances, which is clearly seen for LMC or SMC objects in Fig. 21. This relation is followed well by all the M31 PNe (with the exception of precisely one deficient, halo object; Jacoby & Ciardullo 1999), and a similar picture is found for Galactic objects, except for the halo ones again (Henry 1989).

We have aimed at a simple evaluation of the enrichment for neon, as done previously for oxygen. The result is similar: i.e. after a hundred thermal pulses, the surface abundance of neon is substantially increased, and the oxygen-neon correlation is maintained, even with oxygen (and thus neon) production.

The production of neon in the core does not necessarily follow that of oxygen systematically, it is very dependent on the initial mass of the progenitor. The most plausible explanation for the objects lying below the main correlation and in the lower left corner of Fig. 21 is that they have experienced some oxygen production not followed by neon production. Their progenitors are probably of low mass, with low initial metallicities, as also shown by their low argon abundance. Good examples are SMP LMC 5 or SMP LMC 55, which fall on the main correlation in Fig. 23, with low abundances, and show an excess in oxygen. Other objects, such as SMP SMC 1, SMP SMC 16, SMP LMC 2, or SMP LMC 56, show a deficiency in neon without peculiarities in either oxygen or argon, which can be due either to some neon destruction or to a particular initial composition and which needs to be studied in more detail.

Model calculations are clearly desirable for checking the various possibilities in detail. Production of neon in a given range of initial masses is, for instance, foreseen in the models of Marigo et al. (1996) and Marigo (2001), but the details of the relation, the amount produced, and the precise dependence on initial masses, were not explained. More recently, Marigo et al. (2003) had to invoke a significant neon production (with a correlative low efficiency of its destruction mechanism, i.e. a significant reduction in the production of magnesium and neutrons via the ^{22}Ne$(\alpha, n)^{25}$Mg reaction) to reproduce observed abundances in a small sample of Galactic PNe with presumably low, LMC type, initial abundances. Effective production of neon in the He-burning shell is also demonstrated by observations of PG1159 stars (post-AGB stars after a helium-shell flash; Werner et al. 2004). The observational evidence is therefore growing, and theoretical work follows: increased production efficiency at very low metallicity is shown by Herwig (2004). Specific models to reproduce abundances in PG1159 type objects (bare planetary nebulae central stars, Werner & Herwig 2005) show that significant amounts of ^{18}O and ^{22}Ne from the He-burning shell are brought to the surface by the third dredge-up, when the initial stellar mass is below about 1.5 $M_{\odot}$. For higher masses, some of the neon is burned again into magnesium. Recent models by Charbonnel (2005) confirm the production of ^{22}Ne in PNe progenitor stars and show that its abundance is a clue to the efficiency of various processes, including the production of s-process elements, which are unfortunately not easy to measure in PNe. Clearly more models are required, with the specific initial metallicities relevant to the Large, and more importantly the Small, Magellanic Cloud. As is evident, for instance, in Fig. 24 where Marigo's model predictions have been superposed to the observed data, the models of Marigo et al. (2003) with their set of abundances (mostly LMC abundances, or higher) provide too high values compared to the observed range of abundances.

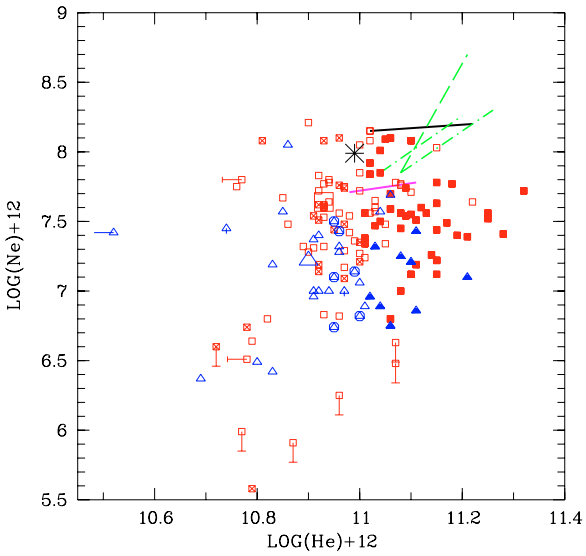

Fig. 24. Relation between neon and helium abundances. The various lines represent model predictions from Marigo et al. (2003); in particular the two continuous, almost horizontal lines are for Galactic and LMC abundances.

4.6. *Initial composition*

Following the above discussions, oxygen cannot be used anymore as a tracer of the initial composition of a PNe progenitor star (nor should neon). Therefore, following a cautionary principle, the only usable elements are those that are believed not to be altered during the various AGB phases, and one should then take their sum to define an "initial metallicity". Among the elements available in our spectra, this therefore leaves only argon and sulfur (but others such as chlorine could be added later). As the accuracy of sulfur abundance determinations is, however, far from satisfactory at the moment, we have no other choice but to use argon alone as the tracer at this stage (even if we are sometimes limited by the faintness of some argon lines). The previous diagrams with argon can thus be used to discuss the evolution and to try to identify objects with peculiar abundances.

We again stress (Fig. 12) the difficulty to make a clear separation between type I and non-type I objects. What is even more interesting is the spread in "total" abundance, showing indeed that the various progenitors did not all start with the same initial abundances. This of course makes the definition of an "enrichment" (and hence the definition of a type I object) the more difficult.

The N/O versus "total" abundance diagram (Fig. 16) helps to clarify this. In this diagram, the nature of what we have called "type i" appears more clearly. While some of them have a "total abundance" that is only marginally different from the classical type I objects (and were therefore omitted from this class only because they are lying close to, but on the "wrong" side of, the border line), the majority of them are, indeed, simply objects with very low initial abundances. Then, although the enrichment in He might be high, it is not enough to make them fall above the He/H limit (which was defined from Galactic objects, and corrected here for the difference in metallicity between the Galaxy and the Clouds, see Paper I) to be called "true" type I objects. This reinforces our claim that the type I PNe in the Clouds can only be defined well once the initial abundance is known, and hence the true relative enrichment can be calculated.

The other diagrams help to select objects of particular interest, either because they have low metallicities, and are then tracers of past chemical composition of the Clouds or because they display signs of oxygen processing (production or destruction) and are key targets for helping refine the models of stellar evolution. If some objects exhibit both low argon and low oxygen (Fig. 17), they are candidates for old, hence low-mass, progenitors. This is the case for SMP LMC 11 (which is also He-poor) and SMP LMC 31, both of type i, and, among the non-type I PNe, we mention MGPN SMC 9, SMP LMC 26 and SMP LMC 94. Finally, SMP LMC 64 is a very peculiar object, with extremely high temperature and density (Dopita et al.1991b), hence with more uncertain abundance determinations.

If objects appear to be weak in oxygen, but not in argon, it is a sign of oxygen destruction. Notable are MGPN SMC 12, SMP SMC 21, SMP SMC 22, SMP SMC 23, and SMP SMC 25, all of them type I or type i. This is consistent with the idea that type I's have high-mass progenitors, where the oxygen destruction is likely to occur.

Objects appearing weak in argon, but not in oxygen are likely to have produced some oxygen. This is the case for SMP SMC 8, SMP SMC 12, SMP SMC 20, or SMP SMC 32 in the SMC; or in the LMC, for SMP LMC 122, SMP LMC 33, SMP LMC 60, SMP LMC 68 or SMP LMC 72. Such objects cannot directly appear as type I's because their relatively high O abundance prevents their N/O to cross the type I limit (even with a limit revised to −0.6 for the Clouds). Yet some of them nevertheless have a (relatively) high He abundance. That objects in the last two categories are more easily identified in the SMC than in the LMC is the consequence of the higher efficiency of the various processes involved (as discussed earlier, and in Paper I) when the initial metallicity is low. Finally, more objects with oxygen processing can be selected from the Ne-O diagram (Fig. 21), for instance MGPN SMC 12, SMP LMC 11, or SMP LMC 26 (oxygen destruction), or SMP SMC 1, SMP SMC 16, SMP LMC 5, SMP LMC 31 or SMP LMC 55 or SMP LMC 56 (oxygen production). LMC 120-N 99 enters in the same category, but being a very low excitation object, the determination of its physical parameters is more uncertain. Those objects will be subject to further observations to refine their diagnostics and derive the properties of their progenitor stars (Leisy & Dennefeld, in preparation).

5. Spatial distribution and chemical evolution

This very large sample of objects (156 good spectra out of 183 PNe) should allow us to check the chemical homogeneity of the Clouds much better than with H II regions, where only about 20 abundance determinations are available. We plot the spatial distribution of our "total" abundances (in this case, argon only) in Figs. 25 and 26 for the LMC and the SMC, respectively. We see that contrary to the common assumption derived from the H II regions, the abundances seen in the Magellanic Clouds are not homogeneously distributed, and the type I's do not correlate with known regions of recent SF. Neither in the LMC nor in the SMC.

Even if we only consider the type I PNe, whose abundances should, owing to their young age, reflect a value close to present abundances, comparable to H II regions, the Clouds do not appear well-mixed. In the SMC, the abundances seem to divide into two zones: one in the South-West with higher values, and one in the North-East with lower ones. This would be consistent with a younger age for the south western part of the SMC bar, but somewhat in contradiction with the recent idea that SF has proceeded rather continuously in the SMC over the past 10 billion years or so (Van den Bergh 1990), a period of time longer than the age of the oldest PN progenitor.

For the LMC, the situation is more complicated. Low-abundance objects seem to be distributed well over the surface of the galaxy, such as a halo-type population. However, PNe with low mass progenitors would, in their vast majority, trace SF in an age interval of only about 0.5 to 10 billion years ago, which corresponds to a period where the stellar formation in the LMC, as determined by cluster metallicities, was believed to be close to zero (Da Costa 1991).

However, this contradiction is only apparent as studies of field stars (instead of clusters) show that SF was going on

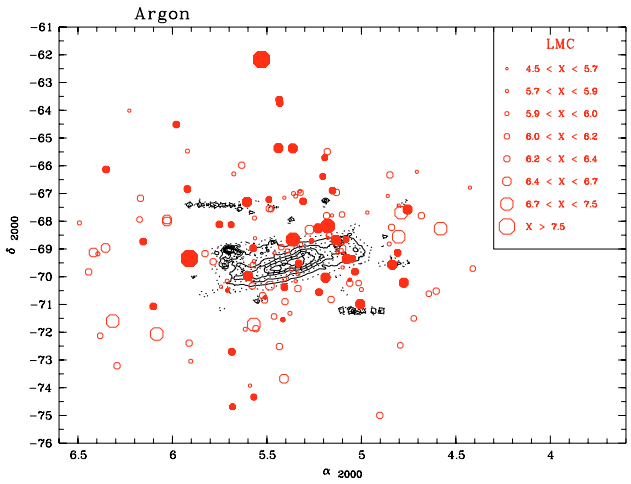

Fig. 25. The spatial distribution of PNe argon abundances in the LMC. Each PN is represented by a circle, size whose is proportional to the total abundance. Filled symbols represent type I PNe.

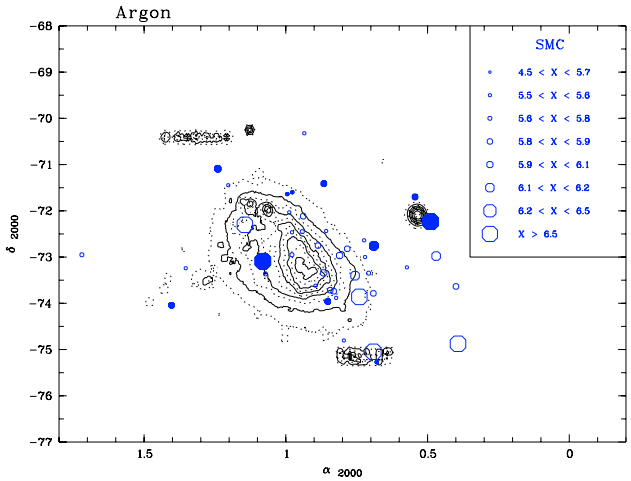

Fig. 26. Same as Fig. 25, but for the SMC.

rather continuously in the past, with a marked increase around 4 billions years ago (Van den Bergh 1990), so that the PNe could help determine the intensity of this SF "renewal". One would expect more objects with very low metallicities, well-distributed over the "halo", but this is certainly an observational bias, as those PNe are old and faint and have not been observed in large numbers with 4 m class telescopes. They are clear targets for larger telescopes.

The higher abundances in PNe seem to be more confined to the bar and south eastern region, not correlated with sites of recent SF as seen from the H II regions. However, as H II regions only trace the very massive stars, this could be consistent with the idea that SF is proceeding by bursts and rapidly migrating from one place to another. The PNe with high abundances would then trace regions of "relatively recent" SF, that is, places where the SF has been active recently, but is not ongoing. Indeed, when looking at the enrichment produced by PNe, with the spatial distribution of N/O (Figs. 27 and 28), it is apparent that type I PNe are distributed uniformly, so that "recent" SF was proceeding throughout the Clouds. The necessary test for the chemical homogeneity, both in space and time, is to compare the abundances derived from a given PN with those derived from an H II region

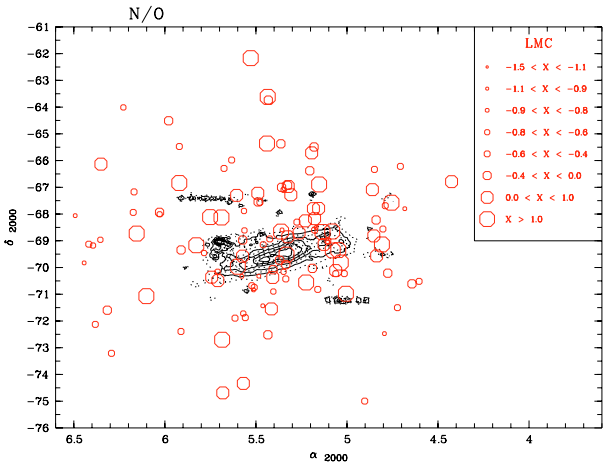

Fig. 27. Spatial distribution of N/O in LMC, as measured in PNe. The size of the symbol increases with N/O value (details in the insert).

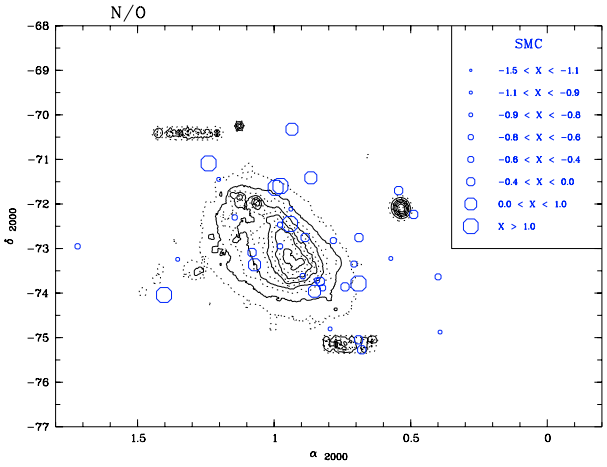

Fig. 28. Same as Fig. 27, but for the SMC.

located in the same physical region. More H II regions therefore need to be observed.

6. Conclusions

We have presented new spectra of 65 Planetary Nebulae in the Magellanic Clouds, for which abundances were derived. We reanalyzed published data of other PNe in the same way to produce a homogeneous sample of abundances for 183 PNe in both Clouds, out of which 156 have been finally retained for further analysis, being considered as having good quality data. This large sample allows us to highlight several observational facts for the first time through analysis of classical abundance-abundance diagrams. We have arrived at the following conclusions:

- There is a continuity in He and N/O between type I's and non-type I PNe, so that the distinction between the two types becomes difficult.
- The third dredge-up is taking place in most objects (as discussed in Paper I).
- The Hot Bottom Burning takes place in the most massive objects, leading to high N/O values.
- Overshooting seems to be active and is a good way to explain the observed enhanced oxygen abundance: it leads to a large oxygen production in the core, later released during the thermal pulses. Inclusion of rotation in models seems, however, to strongly affect the oxygen production, too, especially at low metallicities.
- Many reactions are more efficient at lower initial metallicities. This is true for the HBB, which then takes place in lower mass stars (as seen in the SMC). It is true for the 3rd dredge-up, taking place in nearly all stars in the SMC, 50% of them in the LMC and only a small fraction in our Galaxy. It is true for oxygen destruction or production, not seen in our Galaxy, but seen in the LMC and even more in the SMC.
- Abundances of oxygen and neon in PNe envelopes appear to be affected by internal processing and do not reflect, contrary to what was believed earlier, the initial abundances of the progenitor star.

As a consequence, neither oxygen nor neon should be used to trace the chemical history of a galaxy when using PNe. Chlorine, sulfur, or argon, which should not be affected by processing in the PNe progenitor star, should instead be used to measure the initial abundances of the progenitor. Unfortunately the first element, chlorine, has very weak emission lines, and in no object in LMC or SMC is the [Cl III] doublet even detected. The abundance of the second, sulfur, is presently not well-determined, because some of the lines of the dominant ions are too weak, or they fall outside the classical optical range thereby making the uncertainty in the final abundance very large.

As a result only argon is presently suitable and it is used as the indicator for the "initial metallicity" of PNe progenitor stars, instead of an average of several different elements. Observations of some of the brighter PNe with larger telescopes to measure fainter lines and an extension into the IR (to measure additional ionization stages of elements) should help to overcome this limitation. Similarly, access to the UV range is needed to obtain abundances of elements such as C, which play a key-role in understanding on-going processes. It should also be noted that a fair fraction of already published spectra are of poor quality, often not allowing even for a proper temperature or density determination. This increases the scatter in the diagrams and reduces the ability to interpret some of the observed effects. An observational effort to secure more high-quality spectra is therefore appropriate. Some effort for fainter objects (fluxes less than 100×10^{-16} erg cm^{-2} s^{-1}) would at the same time reduce the existing bias in favor of brighter (higher mass?) objects. This, together with observations of some isotopic ratios whenever possible (such as ^{12}C/^{13}C), would then allow finer comparison between observed abundances and stellar evolution predictions and fully exploit the potential of PNe as tracers of the chemical evolution in Local Group galaxies.

Acknowledgements. P.L. would like to thank his parents for hospitality and support during a critical period between the start of this work several years ago and its final completion. M.D. acknowledges ESO's support, through its short-term visitor program in Chile, where part of this work was completed. We thank the referee for useful comments that helped to improve the clarity of this paper.

Appendix A: Fluxes

We present here the tables of intensities for all 65 PNe observed by us. For completion, all objects are listed, including those already discussed in Paper I. In addition, for practical reasons, to show what intensities were used in our new, homogeneous, abundance determinations, we present intensities also for the full sample (183 objects), all in the same format.

These tables are available only in electronic form at the CDS.

References

Allende Prieto, C., Lambert, D. L., & Asplund, M. 2001, ApJ, 556, 63
Becker, S. A., & Iben, I., Jr. 1979, ApJ, 232, 831
Becker, S. A., & Iben, I., Jr. 1980, ApJ, 237, 111
Bono 2000, Private communication
Charbonnel, C. 2005, PNe as astronomical tools, Gdansk conference, ed. R. Szczerba, G. Stasińska, & S. K. Górny, AIP Conf. Ser., in press
Costa, R. D. D., de Freitas Pacheco, J. A., & Idiart, T. P. 2000, A&AS, 145, 467
Da Costa, G. S. 1991, The Magellanic Clouds, ed. R. Haynes, & D. Milne, IAU Symp., 148, 183
Dennefeld, M. 1989, Recent developments of Magellanic Clouds research, ed. K. S. de Boer, F. Spite, & G. Stasinska, 107
Dennefeld, M., & Stasinska, G. 1983, A&A, 118, 234
Dopita, M. A., & Meatheringham, S. J. 1990, ApJ, 357, 140
Dopita, M. A., & Meatheringham, S. J. 1991a, ApJ, 367, 115
Dopita, M. A., & Meatheringham, S. J. 1991b, ApJ, 374, L21
Dufour, R. J. 1984, Structure and evolution of the MC's, ed. S. van den Bergh, & K. S. de Boer, IAU Symp., 108, 353
Garnett, D. R. 1999, New views of the Magellanic Clouds, ed. Y. H. Chu, N. B. Suntzeff, J. E. Hesser, & D. A. Bohlender, IAU Symp., 190, 266
Grevesse, N., & Anders, E. 1989, Cosmic Abundances of Matter, ed. C. J. Waddington, AIP Conf. Proc., 183, 1
Groenewegen, M. A. T., & de Jong, T. 1993, A&A, 267, 410
Henize, K. G. 1956, ApJS, 2, 315 (LHA-Nxx)
Henry, R. B. C. 1989, MNRAS, 241, 453
Herwig, F. 2000, A&A, 360, 952
Herwig, F. 2004, ApJS, 155, 651
Hill, V., Francois, P., Spite, M., et al. 2000, A&AS, 364, L19
Iben, I. 1977, ApJ, 217, 788
Iben, I., & Truran, J. W. 1978, ApJ, 220, 980
Iben, I., & Renzini, A. 1983, ARA&A, 21, 271
Jacoby, G. H., & Ciardullo, R. 1999, ApJ, 515, 169
Kaler, J. B., Iben, I., Jr., & Becker, S. A. 1978, ApJ, 224, 63
Kingsburgh, R. L., & Barlow, M. J. 1994, MNRAS, 271, 257
Leisy, P., & Dennefeld, M. 1996, A&AS, 116, 96 (Paper I)
Leisy, P., & Dennefeld, M. 2000, Rev. Mex. Astron. Astrofis., 9, 227
Marigo, P., Bressan, A., & Chiosi, C. 1996, A&A, 313, 545
Marigo, P. 2001, A&A, 370, 194
Marigo, P., Bernard-Salas, J., Pottasch, S. R., et al. 2003, A&A, 409, 619
Meatheringham, S. J., & Dopita, M. A. 1991a, ApJS, 75, 407 (Paper a)
Meatheringham, S. J., & Dopita, M. A. 1991b, ApJS, 76, 1085 (Paper b)
Meatheringham, S. J., Dopita, M. A., Ford, H. C., & Webster, B. L. 1988, ApJ, 327, 651
Metcalfe, T. S., Salaris, M., & Winget, D. E. 2002, ApJ, 573, 803
Miller, J. S., & Matthews, W. G. 1972, ApJ, 172, 593
Monk, D. J., Barlow, M. J., & Clegg, R. E. S. 1988, MNRAS, 234, 583
Morgan, D. H. 1994, A&AS, 103, 235 (M94b-xx)
Morgan, D. H. 1995, A&AS, 112, 445 (M95-x)
Morgan, D. H., & Good, A. R. 1985, MNRAS, 213, 491 (MGPN SMC xx)
Morgan, D. H., & Good, A. R. 1992, A&AS, 92, 571 (MGPN LMC xx)
Nandy, K., Morgan, D. H., Willis, A. J., et al. 1981, MNRAS, 196, 955
Peimbert, M. 1978, Planetary Nebulae, ed. Y. Terzian (Dordrecht: Reidel), IAU Symp., 76, 215
Peimbert, M. 1984, Structure and Evolution of the MC's, ed. S. van den Bergh, & K. S. de Boer, IAU Symp., 108, 363
Peimbert, M. 1985, Rev. Mex. Astron. Astrofis., 10, 125
Renzini, A., & Voli, M. 1981, A&A, 94, 175
Ratag, M. A., & Pottasch, S. R. 1990, A&A, 227, 207
Sanduleak, N., MacConnell, D. J., & Phillip, A. G. D. 1978, PASP, 90, 621 (SMP LMC (or SMC) xxx)
Spite, F., & Spite, M. 1991, The Magellanic Clouds, ed. R. Haynes,& D. Milne, IAU Symp., 148, 243
Stanghellini, L., Shaw, R. A., Balick, B., & Blades, J. C. 2000, ApJ, 534, L167
Sweigart, A. V., Greggio, L., & Renzini, A. 1989, ApJS, 69, 911
Sweigart, A. V., Greggio, L., & Renzini, A. 1990, ApJ, 364, 527
Van den Bergh, S. 1999, New views of the Magellanic Clouds, ed. Y. H. Chu, N. B. Suntzeff, J. E. Hesser, & D. A. Bohlender, IAU Symp., 190, 569
Vassiliadis, E., & Wood, P. R. 1993, ApJ, 413, 641
Vassiliadis, E., Meatheringham, S. J., & Dopita, M. A. 1992, AJ, 394, 489
Werner, K., & Herwig, F. 2005 [arXiv:astro-ph/0512320]
Werner, K., Rauch, T., Reiff, E., et al. 2004, A&A, 427, 685
Whitford, A. E. 1958, AJ, 63, 201